# Pulse-and-Glide Operations for Hybrid Electric Vehicles in the Car-Following Scenario

Su-Yang Shieh, Tulga Ersal, and Huei Peng

*Abstract*—This paper is focused on the pulse-and-glide (PnG) control for a parallel hybrid electric vehicle (HEV) in car-following. PnG is an eco-driving technique that alternately turns on and off the engine to save fuel. For HEVs, the ride comfort concerns by PnG in conventional vehicles can be alleviated by oscillating the battery state of charge (SOC), instead of the vehicle speed. However, due to the ohmic losses during the battery charging and discharging process, the fuel saving potential is much reduced. In order to reach a balance between ride comfort and fuel economy, a control method is proposed to utilize both the vehicle body and the battery as the energy buffers simultaneously in the PnG operation. In particular, two minimum-time control problems, one for the pulsing phase and another for the gliding phase, are formulated and implemented as model predictive control (MPC). With the applications of a series of approximations and sparsity optimization techniques, these two control problems become quadratic programming (QP) problems after the application of the pseudo-spectral (PS) method. The online implementability is thus ensured. Numerical simulations using naturalistic driving data show on average 17.1% and 5.1% improvements of fuel economy for local and highway speeds, respectively. It is shown that the proposed method is able to improve the fuel economy while maintaining both ride comfort and SOC sustenance.

*Index Terms*—hybrid electric vehicles, eco-driving, pulse-and-glide, model predictive control.

## NOMENCLATURE

| | |
|---|---|
| $A_v$ | Vehicle frontal area. |
| $a$ | Acceleration of the ego (following) vehicle. |
| $a_{\text{ACC}}$ | Acceleration control input of the adaptive cruise control (ACC) method for benchmark. |
| $a_b$ | Braking acceleration, less or equal to zero. |
| $a_{\text{CACC}}$ | Acceleration control input of the cooperative adaptive cruise control (CACC) method for benchmark. |
| $a_{\text{lim}}$ | Acceleration limit for ride comfort. |
| $a_P$ | Acceleration of the preceding vehicle. |
| $\alpha$ | Positive constant for defining $w(t)$, the increasing function used in the sparsity optimization for minimum-time MPC. |
| $C_{\text{bat}}$ | Battery capacity. |
| $C_d$ | Air drag coefficient. |
| $c_{\omega v}$ | Constant showing the relation between motor speed and vehicle speed, equal to $\omega_m/v$. |
| $d_0$ | Standstill range used in the range policy. |

| | |
|---|---|
| $d_{\text{lim}}$ | Deceleration limit for ride comfort. |
| $dR$ | Range error. |
| $\delta_v$ | Normalized speed deviation from the average speed in PnG, equal to $(v-\bar{v})/\bar{v}$. |
| $\Delta E_k$ | Kinetic energy difference of the vehicle between the maximum and minimum speed. |
| $\Delta T$ | MPC time step. |
| $\Delta T_{\text{gld}}$ | MPC horizon for the gliding phase problem. |
| $\Delta T_{\text{pls}}$ | MPC horizon for the pulsing phase problem. |
| $E_{r,\text{add},i}$ | Additional energy loss by road load due to speed oscillation from Speed-PnG. |
| $\varepsilon_v$ | Error to the target speed. |
| $\varepsilon_{\text{soc}}$ | Error to the target SOC. |
| $\eta_m$ | Motor efficiency. |
| $\eta_{\text{bat},i}$ | Battery efficiency in charging ($i = \text{ch}$) and discharging ($i = \text{disch}$). |
| $\eta_T, \eta_0$ | Gear efficiency of transmission and final drive. |
| $\eta_{\text{vb},i}$ | Efficiency of vehicle body as energy buffer in gliding phase ($i = \text{gld}$) and pulsing phase ($i = \text{pls}$). |
| $f_r$ | Rolling resistance coefficient. |
| $g$ | Acceleration of gravity. |
| $h_\tau$ | Time headway. |
| $I_{\text{bat}}$ | Battery current. |
| $k_1$ | Constant associated with aerodynamic drag, equal to $-C_d\rho_a A_v/(2M_v)$, parameters in Table I. |
| $k_2$ | Constant associated with transmission, equal to $\eta_T\eta_0 r_T r_0/(M_v r_w)$, parameters in Table I. |
| $K_P, K_D$ | Proportion and derivative gains of the proportional-derivative (PD) control of the benchmark method. |
| $M_v$ | Vehicle weight. |
| $P_{\text{bat}}$ | Battery power. |
| $P_m$ | Motor power. |
| $Q_{\text{CS}}, Q_{\text{PnG}}$ | Fuel rate of constant-speed driving and pulse-and-glide with engine. |
| $R$ | Range to the preceding vehicle. |
| $R_{\text{des}}$ | Desired range to the preceding vehicle. |
| $R_{\text{bat}}$ | Battery inner resistance. |
| $r_T, r_0$ | Gear ratio of transmission and final drive. |
| $r_w$ | Effective tire radius. |
| $\rho_a$ | Air density. |
| $s_a, s_d$ | Slack variables for acceleration and deceleration constraints. |
| $SOC$ | Battery state of charge. |
| $t_{0,i}, t_{f,i}$ | Initial and final time of the pulsing ($i = \text{pls}$) and gliding ($i = \text{gld}$) phase. |

Corresponding author: Su-Yang Shieh. The authors are with the Department of Mechanical Engineering, University of Michigan (e-mail: syshieh@umich.edu, tersal@umich.edu, hpeng@umich.edu)

| $t_c$ | Initial time in the MPC problems (current time). |
| $T_e$ | Engine torque. |
| $T_m$ | Motor torque. |
| $\bar{T}_{sw}$ | Most efficient engine torque at average speed, $\bar{v}$. |
| $v$ | Speed of the ego (following) vehicle. |
| $\bar{v}$ | Average speed for PnG. |
| $v_P$ | Speed of the preceding vehicle. |
| $V_{oc}$ | Battery open-circuit voltage. |
| $w(t)$ | Increasing function of time. |
| $w_a$ | Weighting factor in the pulsing phase problem. |
| $w_b, w_d$ | Weighting factors in the gliding phase problem. |
| ACC | Adaptive cruise control. |
| CACC | Cooperative adaptive cruise control. |
| CAFE | Corporate Average Fuel Economy standards. |
| CS | Constant speed. |
| CVT | Continuous variable transmission. |
| DP | Dynamic programming. |
| EV | Electric vehicle |
| FV | Following vehicle. |
| HEV | Hybrid electric vehicle. |
| ICE | Internal combustion engine. |
| LGR | Legende-Gauss-Radau. |
| MPC | Model predictive control. |
| MPG | Miles per gallon. |
| NHTSA | National Highway Traffic Safety Administration. |
| OCV-R | Open-circuit-voltage-resistance. |
| PnG | Pulse-and-glide. |
| PD | Proportional-derivative. |
| PV | Preceding vehicle. |
| QP | Quadratic programming. |
| SOC | State of charge. |
| PS | Pseudo-spectral. |

# I. Introduction

**T**HE Corporate Average Fuel Economy (CAFE) standards in the U.S. require the original equipment manufacturers to improve fuel economy of their production vehicles continuously. According to National Highway Traffic Safety Administration (NHTSA) in 2022, an industry-wide fleet average of 49 MPG will be required for passenger cars and light trucks in model year 2026 [1]. Eco-driving, with the advancement of vehicle automation, is a promising research direction to further improve fuel economy, in addition to the efforts that involve new hardware design over the past decades.

In 1976, an eco-driving technique exploiting the characteristics of internal combustion engines (ICEs) by periodic control has been introduced [2]. Later on, this technique has been called pulse-and-glide (PnG) due to the resultant speed increase and decrease [3]. This technique enforces the engine to be operated at efficient points once it is turned on and is commonly used in super-mileage competitions [4]. The concept of PnG operation is shown schematically in Fig. 1. For general ICEs, the fuel-rate curve against output power appears in the concave-convex shape, which enables the fuel saving of PnG. In Fig. 1, the blue square marks the fuel rate for a fixed
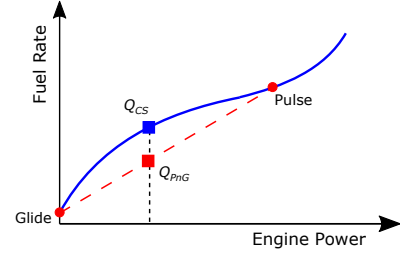


Fig. 1: The mechanism of PnG for fuel saving. The fuel rate of constant-speed driving and that of PnG on average are denoted by $Q_{CS}$ and $Q_{PnG}$, respectively. Due to concavity, $Q_{PnG}$ is below $Q_{CS}$, so the fuel consumption is reduced.

engine operating point that maintains a given constant vehicle speed. Instead of using the fixed engine operating point, in PnG the pulsing and gliding operating points indicated by red dots in Fig. 1 are used alternately. The pulsing and gliding points correspond to operating the engine at the most efficient point and turning off the engine, respectively. Therefore, the engine is turned on and off alternately in PnG. With engine on/off transients and variation of road load ignored, the average fuel rate by using PnG is the red square for maintaining the same vehicle speed. The red square is lower than the blue square, so lower fuel consumption is possible. Therefore, the concave region of the curve suggests a lower average fuel rate is achievable by switching between the pulsing and gliding points. The concavity of this region depends on the engine characteristics. The more concave this region is, the higher the fuel saving potential of PnG is.

Researchers have shown the promising fuel saving performance in literature. Reference [3] presents the simulations of PnG on a 2007 Ford Focus and a 2004 Toyota Prius. The dynamometer experiment using a 2004 Toyota Prius is also presented in [3]. The simulations show 30 to 77% MPG improvement for the Focus and 24 to 90% for the Prius at low speeds (25 to 35 mph), and a 4% reduction of MPG improvement is observed from the dynamometer result. In [5], researchers show that PnG achieves 15% to 35% fuel saving from 22 mph to 67 mph in simulation. In [6], up to 20% fuel economy improvement is achieved for a vehicle with continuous variable transmission (CVT) in simulations using a rule-based control to determine the PnG switching times. From [5] and [6], the general trend of reduced fuel saving potential with speed increase is pointed out. Later on in [7], the rule-based control in [6] is extended to vehicles with step-gear transmissions and up to 8.9% fuel saving in naturalistic traffic flow is observed from simulations. Reference [8] formulates the optimal control problem in the speed-acceleration domain (rather than the time-speed domain) to determine the PnG strategy for ICE vehicles, and 3% to 5% fuel saving on highways is obtained from simulations. In the real driving experiment of [9], 43.4% improvement of fuel consumption around 40 kph for a Nissan X-trail is obtained via PnG.

On the other hand, Ref. [10] utilizes the Bittanti's $\pi$-test [11], a tool to estimate the performance of periodic control against constant control inputs, to study the mechanism of PnG. Also, in [10] the theoretical basis showing that PnG is

optimal in the concave region of the fuel-rate curve in Fig. 1 is constructed. Reference [12] analyzes the most efficient pulsing operating point for ICE vehicles with CVT. It concludes that an operating point with lower torque and lower rotational speed than the minimum brake specific fuel consumption (BSFC) point is most fuel-economical.

In addition to the papers focusing on PnG directly, some others observe the PnG-like behavior in the control strategies developed. In [13], a stochastic dynamic programming problem for minimizing the fuel consumption is formulated to determine the control policies of the following vehicle (FV). The solutions show the emergent PnG behavior if the following range is relaxed to be within the upper and lower bounds. In [14], a model predictive controller (MPC) with relaxed car-following range is developed and the PnG control shows as the solution. Similarly, in [15] for heavy-duty vehicles, a look-ahead adaptive cruise controller with adjusted car-following distance considering road grade results in alternating phases of throttling (pulsing) and freewheeling (gliding) to save fuel. In [16], a closed-form solution to the optimal control problem for efficient driving is derived based on the Pontryagin's maximum principle. This solution suggests that the PnG operation can reduce the fuel consumption during cruising. Reference [17] proposes a real-time eco-driving mode advice system based on an event-triggered MPC using predictive road and traffic information, the solution of which recommends PnG as the optimal driving mode in cruising.

The above papers are focused on ICE vehicles. Reference [18], instead, establishes two artificial neural networks to decide the eco-driving mode for parallel hybrid electric vehicles (HEVs) based on the upcoming trip in the prediction horizon. The PnG operation is also identified as the driving mode in cruising scenarios. However, detailed controls of engine and motor and the power allocation between them are not discussed in [18]. In [19], the energy-efficient driving profiles for electric vehicles (EVs) are studied using dynamic programming (DP). The DP solutions show the forms of PnG for EVs as well. Reference [20] focuses on PnG in EVs also and proposes a PnG-driven cruise control from intelligent genetic algorithm and particle swarm optimization.

Conceptually, in ICE vehicles, PnG saves fuel by operating the engine at more efficient points when it is turned on. The surplus engine power beyond necessary for maintaining the constant speed is temporarily stored at the vehicle body in the form of kinetic energy. The bimodal operation of PnG, although leads to fuel saving, also causes an oscillation of vehicle speed, which can be detrimental to ride comfort. This concern could be alleviated in HEVs, since the batteries of HEVs can serve as another temporary storage devices for engine power and the speed oscillation can be avoided by using the batteries. In [21], Speed-PnG and SOC-PnG are used to term the PnG operations with vehicle body and battery as the energy buffer, respectively. However, it is pointed out in [21] that the fuel saving potential of SOC-PnG is much lower compared with that of Speed-PnG. Apparently, a trade-off between ride comfort and fuel saving needs to be considered in PnG operations for HEVs.

Some works in the literature focus on the ride comfort of PnG. Based on the Pontryagin's maximum principle, Ref. [22] proposes an approach to determine the period of Speed-PnG that satisfies the jerk level requirement. However, the requirement of vehicle acceleration and deceleration for ride comfort is not considered. Using the comfort index established from the experiment with different participants in [23], the topic of ride comfort and fuel saving from Speed-PnG is studied in [24], of which both jerk and acceleration are considered. The suggested set of requirements for ride comfort is an acceleration less than $0.3$ m/s$^2$ and a jerk between $-6$ to $4$ m/s$^3$, which corresponds to the level of "noticeable only to skeptical customers." Reference [24] quantifies the fuel saving potential with ride comfort considered via numerical simulations, but a control method to fulfill the ride comfort in PnG is not proposed.

In light of the literature review above, a significant challenge is identified; namely, a control framework for PnG that can effectively consider ride comfort limits for fuel saving does not exist. This challenge is important to address, because poor ride comfort will prevent the adoption of PnG technology. This paper aims to address this challenge by synergistically combining Speed-PnG and SOC-PnG, i.e., exploiting both the vehicle body and the battery as the energy buffers at the same time, to reach a balance between fuel saving and ride comfort.

To this end, two optimal control problems are formulated, one for the pulsing phase and another for the gliding phase. Based on the features of the motor and engine maps, these two problems are formulated as minimum-time control problems, which lead to efficient problem-solving while applying the sparsity optimization approach introduced in [25]. For ride comfort, only the levels of acceleration and deceleration are considered for the sake of maintaining a smaller size for the optimal control problems formulated. Jerks, especially those happening at the moments of PnG switching, are assumed to be limited by the low-level actuator controllers. The design of these low-level controls of the motor and engine is out of the scope of this paper. To achieve online implementability, the vehicle dynamics and battery dynamics are linearized. The bilinear term of motor power in the linearized battery dynamics is convexified by the McCormick envelope [26]. Then after being transcribed by the pseudo-spectral (PS) method, both the pulsing and gliding phase problems become quadratic programming (QP) problems, which can be solved efficiently with existing solvers.

The work presented here is based on the authors' previous conference paper [27]. As opposed to the conference version, in which the pulsing and gliding phase problems are solved as boundary-value problems, in this paper a minimum-time approach is proposed. With this minimum-time control formulation, the final-time searching algorithm designed for finding the PnG switching time in [27] is not needed. This way, the need for a good initial guess for switching time to obtain good performance is eliminated. Furthermore, the constraints are modified so that the convergence performance is improved, allowing a better PnG performance when following a preceding vehicle (PV) that varies its speed. In addition, the proposed method is applied to naturalistic driving scenarios, where the PV travels with the speed trajectories from the Safety Pilot
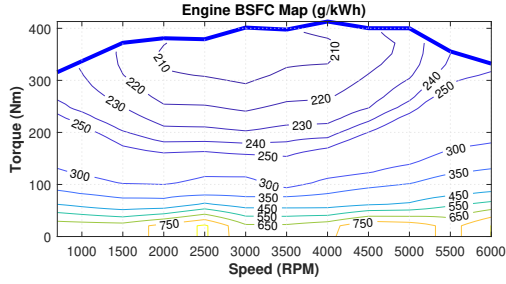
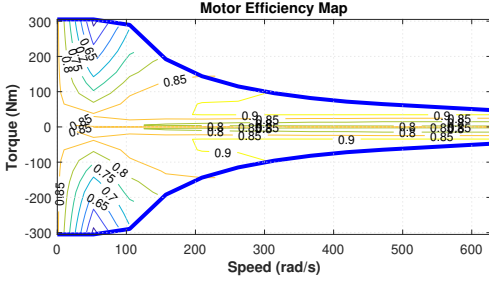Fig. 2: The engine BSFC map. The thick blue line indicates the maximum torque at different engine speeds.



Fig. 3: The motor efficiency map. The thick blue lines indicate the maximum charging and discharging torque at different motor speeds.



Fig. 4: The open circuit voltage and inner resistance of the battery pack.

TABLE I: Vehicle Parameters.

| Parameter | Description | Value | Unit |
|-----------|-------------|-------|------|
| $M_v$ | vehicle weight | 2948 | kg |
| $C_d$ | air drag coefficient | 0.4 | - |
| $A_v$ | vehicle frontal area | 3.26 | $m^2$ |
| $\rho_a$ | air density | 1.202 | $kg/m^3$ |
| $f_r$ | rolling resistance | 0.015 | - |
| $r_w$ | effective tire radius | 0.3848 | m |
| $g$ | acceleration of gravity | 9.81 | $m/s^2$ |
| $r_T$ | gear ratio (gear 1-6) | [4.03, 2.36, 1.53, 1.15, 0.85, 0.67] | - |
| $\eta_T$ | gear efficiency (gear 1-6) | [0.963, 0.971, 0.993, 0.993, 0.995, 0.993] | - |
| $r_0$ | final drive ratio | 3.23 | - |
| $\eta_0$ | final drive efficiency | 0.966 | - |
| $C_{\text{bat}}$ | battery capacity | 6 | kWh |

dataset [28] in car following. The statistical results of 17.1% and 5.1% MPG improvements for local and highway speeds are obtained via numerical simulations. Therefore, the refined method proposed in this paper is more amenable to real-world implementations.

The rest of this paper is organized as follows. In Sec. II, the vehicle model used in this study is introduced. In Sec. III, the discussion of efficiency of vehicle body and battery as different energy buffers is presented. The problem formulation and solution strategy are presented in Sec. IV. The simulation results are shown in Sec. V. Lastly, the conclusions are drawn in Sec. VI.

## II. VEHICLE MODEL

The vehicle focused on in this paper is a parallel HEV with a step-gear transmission. The key parameters of it are in Table I. The engine BSFC map and the motor efficiency map are shown in Fig. 2 and Fig. 3, respectively. In the following, the vehicle and SOC dynamics are described.

### A. Vehicle Dynamics

Only the longitudinal vehicle dynamics is considered, and the vehicle is modeled as a point mass. The constant time headway range policy is adopted for car following:

$$R_{\text{des}} = d_0 + h_\tau v_P, \tag{1}$$

where $R_{\text{des}}$ is the desired range to the PV, $d_0$ is the standstill range, $h_\tau$ is the time headway, and $v_P$ is the speed of PV. The dynamics of range error $dR := R - R_{\text{des}}$, where $R$ is the range to the PV, is

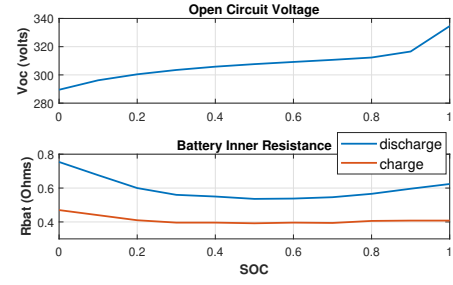$$d\dot{R} = -v + v_P + h_\tau a_P, \tag{2}$$

with $a_P$ being the acceleration of PV. The dynamics of FV speed is

$$\dot{v} = k_1 v^2 + k_2(T_e + T_m) - g f_r, \tag{3}$$

where $k_1 := -C_d \rho_a A_v/(2M_v)$ and $k_2 := \eta_T \eta_0 r_T r_0/(M_v r_w)$. The parameters $C_d$, $\rho_a$, and $A_v$ are the air drag coefficient, the air density, and the vehicle frontal area, respectively. The transmission gear ratio and the associated gear efficiency are labelled with $r_T$ and $\eta_T$, respectively. Similarly, $r_0$ is the final drive ratio and $\eta_0$ is the efficiency of final drive. $M_v$ is the vehicle weight and $r_w$ is the effective tire radius. The road is assumed to be flat. The rolling resistance is composed of the acceleration of gravity $g$ and the rolling resistance coefficient $f_r$. $T_e > 0$ is the engine torque, and $T_m$ is the motor torque. $T_m > 0$ means that the motor is providing driving power from the battery (discharging), while $T_m < 0$ corresponds to battery charging.

### B. SOC Dynamics

The open-circuit-voltage-resistance (OCV-R) model is adopted for the SOC dynamics:

$$\dot{SOC} = \frac{-I_{\text{bat}}}{C_{\text{bat}}} = -\frac{V_{\text{oc}} - V_{\text{oc}}\sqrt{1 - 4P_{\text{bat}}R_{\text{bat}}/V_{\text{oc}}^2}}{2R_{\text{bat}}C_{\text{bat}}}, \tag{4}$$

where $C_{\text{bat}}$, $R_{\text{bat}}$, and $V_{\text{oc}}$ are respectively the capacity, the inner resistance, and the open-circuit voltage of the battery pack. The battery power $P_{\text{bat}}$ in (4) is related to the motor power $P_m$ as $P_{\text{bat}} = \eta_m P_m$ while charging and $P_{\text{bat}} = \eta_m^{-1} P_m$ while discharging, with $\eta_m$ the motor efficiency from Fig. 3. The open-circuit voltage and the battery inner resistance are from Fig. 4, as functions of SOC.
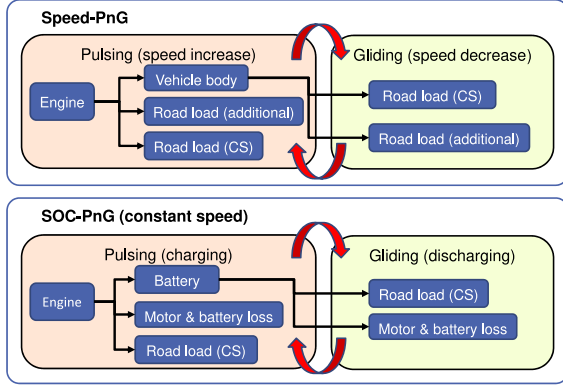
Fig. 5: The schematics of energy flow for Speed-PnG and SOC-PnG.



Fig. 6: The efficiency of vehicle body as the energy buffer with 10% speed oscillation.

## III. Energy Buffers: Vehicle Body versus Battery

In PnG operations, the engine is operated at more efficient operating points compared with those for constant-speed driving. The surplus engine power beyond maintaining the constant speed can be temporarily stored and later on be used to drive the vehicle when the engine is turned off. For HEVs, we can choose to store the engine power in the vehicle body or in the battery. This section discusses these two energy buffers, namely, the vehicle body in Speed-PnG and the battery in SOC-PnG. Specifically, their efficiency for temporary storage of energy from engine is compared to motivate introducing speed oscillations to SOC-PnG to improve the fuel saving performance.

The vehicle is assumed to be a point mass, so it can be viewed as a perfect energy storage buffer without energy loss. However, the speed oscillation in Speed-PnG increases the road load. This part of additional energy loss due to speed oscillation is thus considered in the efficiency calculation for a fair comparison to SOC-PnG, which is with constant speed.

Figure 5 shows the energy flow for Speed-PnG and SOC-PnG without speed oscillation. In the pulsing phase of Speed-PnG, part of the energy from the engine is stored in the vehicle body as kinetic energy and the rest is dissipated because of road load. Based on the concept above, the energy loss due to road load is further divided into two portions, which are the loss for constant speed driving and the additional loss due to speed oscillation. In the gliding phase, the energy stored in the vehicle body is released to overcome the road load. For SOC-PnG, the energy from the engine charges the battery while maintaining constant speed. Then, the engine is turned off and the battery serves as the power source to drive the vehicle. In this process, SOC-PnG incurs the motor and battery loss due to energy conversions.

Assume a vehicle is conducting Speed-PnG around an average speed $\bar{v}$ with maximum and minimum speed, $v_{\max}$ and $v_{\min}$. The efficiency of vehicle body as an energy buffer in the pulsing and gliding phase is defined respectively as

$$\eta_{\text{vb,pls}} := \frac{\Delta E_K}{\Delta E_K + E_{r,\text{add,pls}}}, \tag{5}$$

and

$$\eta_{\text{vb,gld}} := 1 - \frac{E_{r,\text{add,gld}}}{\Delta E_K}, \tag{6}$$
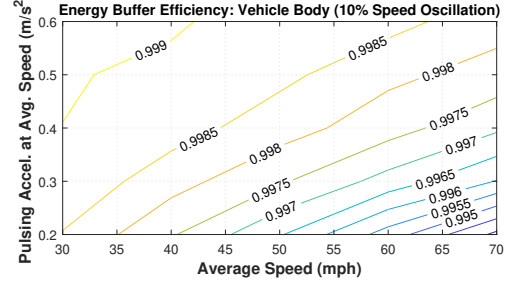
where $\Delta E_K := M_v(v_{\max}^2 - v_{\min}^2)/2$, and $E_{r,\text{add,pls}}$ and $E_{r,\text{add,gld}}$ are the additional energy loss due to speed oscillation by road load in pulsing and gliding phase, respectively. They are defined as

$$E_{r,\text{add},i} := \int_{t_{0,i}}^{t_{f,i}} \frac{1}{2} C_d \rho_a A_v (v^3 - \bar{v}^3) dt, \tag{7}$$

where $i \in \{\text{pls}, \text{gld}\}$ and the integration is with the initial and final time of pulsing or gliding phase. Figure 6 shows the total efficiency of vehicle body in Speed-PnG, i.e., $\eta_{\text{vb,pls}} \cdot \eta_{\text{vb,gld}}$, with 10% speed oscillation under different average speed $\bar{v}$ and pulsing acceleration, using the parameters in Table I. The engine power is assumed to be constant in each case in Fig. 6. The efficiency of vehicle body is above 0.99 in all cases. It means that the additional loss due to speed oscillation by road load is almost negligible.

With the battery model (4), the battery charging and discharging efficiencies of SOC-PnG without speed oscillation are defined respectively as

$$\eta_{\text{bat,ch}} := \frac{V_{\text{oc}}}{V_{\text{oc}} + |I_{\text{bat}}| R_{\text{bat}}}, \tag{8}$$

and

$$\eta_{\text{bat,disch}} := 1 - \frac{I_{\text{bat}} R_{\text{bat}}}{V_{\text{oc}}}. \tag{9}$$

Then, (8) and (9) for different SOC and battery power $P_{\text{bat}}$ is plotted in Fig. 7. The battery efficiency decreases in both charging and discharging as the battery power increases, due to the increased battery current. If the gear efficiency is neglected and the motor efficiency is assumed to be 0.9, the required battery power to maintain constant speed at 40 mph is about 13.6 kW and the battery discharging efficiency is about 0.92 at 0.6 SOC. If the battery charging efficiency is 0.96, the total efficiency of using battery as the energy buffer, with 0.9 motor efficiency, is $0.9 \times 0.92 \times 0.96 \times 0.9 = 0.72$, which is far lower than the efficiency of vehicle body ($> 0.99$).

The conclusion from the above discussion is that the battery is a less efficient energy buffer compared with the vehicle body, mainly because of its multiple energy conversions happening in the process. In battery charging and discharging, energy is converted back and forth between chemical energy and kinetic energy via the form of electrical energy. The total effect is significant even if each conversion is with higher than 0.9 efficiency. Therefore, the vehicle body is a more efficient energy buffer in the PnG operations.
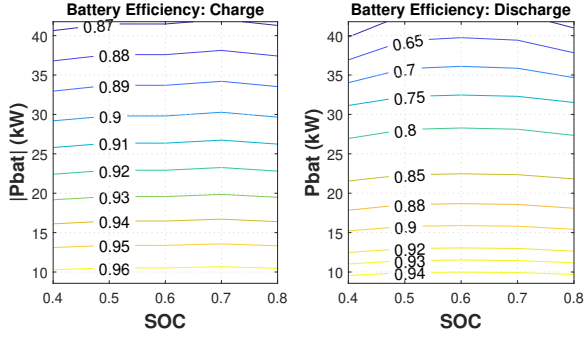
Fig. 7: The efficiency of battery charging and discharging in constant speed SOC-PnG.
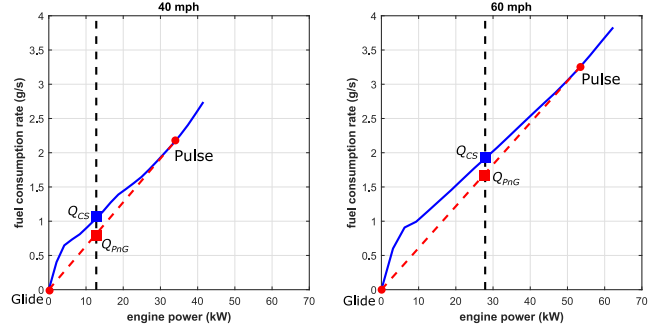


Fig. 8: The fuel-rate curves at 40 mph and 60 mph using gear 6. The fuel-rate curves are obtained by vertically exploring the engine map at the engine speed corresponding to the vehicle speed, 40 mph and 60 mph in these cases. The black dashed lines indicate the required engine power for maintaining the specific speeds. The fuel rate of constant-speed driving and that of PnG on average are denoted by $Q_{CS}$ and $Q_{PnG}$, respectively. The concave-convex shape of the fuel-rate curve is preserved, so the fuel saving potential exists.

## IV. METHODOLOGY

As demonstrated in the last section, the vehicle body is a much more efficient energy buffer compared with the battery. However, pure Speed-PnG would lead to ride comfort concerns. The PnG method proposed in this paper, therefore, is to reach a balance between ride comfort and fuel saving by optimally involving both the vehicle body and the battery as the energy buffers at the same time. The detailed formulation of the pulsing and gliding phase as two separate minimum-time control problems and how to solve them online efficiently as MPC are explained in this section. Also, how the acceleration/deceleration constraints for ride comfort are set using the Safety Pilot dataset is explained. For the case without a PV to follow, the proposed method is still readily usable by assuming there is a virtual vehicle $R_{\text{des}}$ ahead driving at the average speed.

### A. Problem Formulation

It is assumed that the engine can be shut down and disengaged. For the benefits of ride comfort and creating less impact to the traffic, the speed oscillation by PnG is assumed to be small, as 10% in the simulations. Also because of cruising with small speed oscillation, the gear is fixed without shifting in the proposed strategy. Therefore, the fuel saving potentials of PnG can be observed along the vertical lines on the engine map for the corresponding engine speeds. The fuel-rate curves along the vertical lines on the engine map in Fig. 2 for different speeds with different gears are drawn. As examples, the cases of 40 mph and 60 mph with gear 6 are shown in Fig. 8. They also show the similar concave-convex shape as in Fig. 1. As a result, PnG is promising for fuel saving for the vehicle studied here, even if not being able to reach the engine sweet spot because of the step-gear transmission.

Based on the bimodal nature of PnG, the whole problem is formulated as two separate minimum-time control sub-problems, one for each phase. Each sub-problem is with its corresponding PnG target states of range error and speed. In the pulsing phase, the target SOC for charging is also included additionally for SOC sustenance. The detailed formulation of these two sub-problems is as follows.

*1) The Gliding Phase Problem:* In the gliding phase, the vehicle turns off the engine and glides to the preset minimum speed, $v_{\min}$, when it converges to the desired range error, $R_{\text{des}}$.

The motor may need to be turned on to provide the driving force such that the deceleration constraint for ride comfort is not violated in the process. The resultant SOC drop will need to be compensated in the pulsing phase for SOC sustenance. Less battery power consumption thus contributes to better fuel saving for the entire PnG operation. Also, compared with the engine map, the motor map has in general a more uniform efficiency across the operating range. Therefore, with the neglect of motor efficiency variation, the motor driving power is identical to the battery power. In applications, the motor can also be limited to operate within the uniform efficiency region by assigning proper constraints in the formulated problem. This assumption leads to more efficient problem-solving.

Apparently, the battery power consumption during the gliding phase is hinged on the deceleration constraint. With simply enough assist from the motor to satisfy the deceleration constraint, the battery power consumption is minimal and the vehicle will glide to $v_{\min}$ earlier. This leads to formulating the gliding phase problem as the minimum-time control problem for minimizing the overall fuel consumption, as just explained that the battery needs to be charged later on from the engine. One might think that it is desired to maximize the gliding duration to have better fuel saving. However, the gliding phase duration is dictated by the final speed of the pulsing phase. In this situation, the longer the gliding phase is, the higher the price is in term of SOC drop.

The minimum-time control problem for the gliding phase is formulated as follows:

$$
\begin{aligned}
\min_{T_m(t)} \quad & (t_{f,\text{gld}} - t_{0,\text{gld}}) \\
\text{s.t.} \quad & \text{vehicle longitudinal dynamics (2) and (3)} \\
& -d_{\lim} \le a(t) \le a_{\lim} \\
& 0 \le T_m(t) \le T_{m,\max}^{\text{disch}} \\
& \dot{T}_{m,\min} \le \dot{T}_m(t) \le \dot{T}_{m,\max} \\
& dR_{\min} \le dR(t) \le dR_{\max} \\
& v(t_{f,\text{gld}}) = v_{\min}.
\end{aligned}
\tag{10}
$$

As a minimum-time problem, the objective function in (10) is to minimize the time duration of gliding phase $(t_{f,\text{gld}} - t_{0,\text{gld}})$.

The states needs to satisfy the vehicle dynamics. The constraints include those for acceleration and deceleration as ride comfort requirements, the range error constraint for safety, and the limits of motor torque. It is worth noting that the terminal constraint on vehicle speed preclude the trivial solution.

Implemented with the MPC approach, problem (10) is solved every $\Delta T$ s until switching to the pulsing phase. The state values at the current time $t_{0,\text{gld}}$ define the initial boundary conditions of $dR$ and $v$. On the other hand, only the achieving of $v_{\min}$ is included for the final boundary condition, because the vehicle will reach $R_{\text{des}}$ certainly, with the decreased speed slower than the PV due to gliding. This avoids adding too many constraints to problem (10), which might slow down the convergence.

*2) The Pulsing Phase Problem:* The engine is turned on in the pulsing phase. The vehicle accelerates toward the preset maximum speed, $v_{\max}$, while converging to $R_{\text{des}}$ again. Meanwhile, the SOC drop in the gliding phase needs to be restored. In other words, the two energy buffers, the vehicle body and the battery, store the energy from the engine at the same time. The purpose here is to complete the pulsing phase with as efficient engine operating points as possible while satisfying the constraints, especially the acceleration limit for ride comfort. It can be observed from Fig. 2 that for any given engine speed, the engine efficiency is increased with increased torque. This larger engine torque that is more efficient actually lets the vehicle pulse to $v_{\max}$ and complete the battery charging earlier. It leads to the rationale for the minimum-time control formulation for the pulsing phase problem as well. The choice of using efficient operating points of engine is in fact limited by the acceleration constraint for ride comfort, as the most efficient torque at every speed in general generates too high accelerations that may not be ideal for ride comfort in PnG process.

The optimal control problem for the pulsing phase is formulated as follows:

$$\min_{T_m(t),T_e(t)} \quad (t_{f,\text{pls}} - t_{0,\text{pls}})$$

$$\begin{aligned}
\text{s.t.} \quad & \text{vehicle longitudinal dynamics (2) and (3)} \\
& \text{SOC dynamics (4)} \\
& -d_{\lim} \leq a(t) \leq a_{\lim} \\
& T_{m,\max}^{\text{ch}} \leq T_m(t) \leq 0 \\
& \dot{T}_{m,\min} \leq \dot{T}_m(t) \leq \dot{T}_{m,\max} \\
& 0 \leq T_e(t) \leq \bar{T}_{\text{sw}} \\
& \dot{T}_{e,\min} \leq \dot{T}_e(t) \leq \dot{T}_{e,\max} \\
& T_e(t) + T_m(t) \geq 0 \\
& dR_{\min} \leq dR(t) \leq dR_{\max} \\
& v(t_{f,\text{pls}}) = v_{\max} \\
& SOC(t_{f,\text{pls}}) = SOC_{\text{target}}.
\end{aligned} \tag{11}$$

In (11), the time duration of pulsing phase $(t_{f,\text{pls}} - t_{0,\text{pls}})$ is to be minimized based on the minimum-time rationale. Again, the states needs to satisfy the vehicle dynamics. The range constraint and the acceleration/deceleration constraints for ride comfort are still in place. The constraints for engine and motor torques keep these two actuators operating in the desired range. The most efficient engine torque at the given engine speed, $\bar{T}_{\text{sw}}$, is set as the upper limit of engine torque. Since the regenerative braking is not considered in this work, the motor torque for charging the battery is solely from the engine and thus $T_e + T_m \geq 0$ is included. In the pulsing phase, the SOC dynamics is included in the problem formulation. The final condition for SOC is to converge to the target SOC, $SOC_{\text{target}}$. The target SOC is set as the SOC level at the beginning of the gliding phase that immediately precedes the current pulsing phase. Other charging strategy can be easily accommodated as well by assigning $SOC_{\text{target}}$ as appropriate.

Problem (11) is also solved every $\Delta T$ s in the MPC fashion. The state values at the current time $t_{0,\text{pls}}$ define the initial boundary conditions of $dR$, $v$, and $SOC$. For the final boundary conditions, in addition to that for SOC just explained, the achieving of $v_{\max}$ is set without $R_{\text{des}}$ included, because the vehicle will reach $R_{\text{des}}$ surely, with its increased speed higher than that of the PV due to pulsing. This is also due to the intention of reducing the number of constraints for convergence considerations, as in Problem (10). The terminal constraint on vehicle speed once again precludes the trivial solution to this problem.

### B. Solution Strategy

The two sub-problems (10) and (11) are solved using the Legendre PS method with Legende-Gauss-Radau (LGR) collocation points [29]. During the gliding phase, Problem (10) is solved and implemented as MPC until switching to the pulsing phase. Then, during the pulsing phase, Problem (11) is used until switching to the gliding phase again. This process continues alternately as the PnG operation goes. It is worth noting that PnG is by nature discontinuous due to its bimodal operation. Therefore, the multi-interval PS, e.g., [30], needs to be adopted, if the whole PnG cycle is intended to be solved at once. Nevertheless, the two-sub-problem formulation is preferred in the proposed method due to the practicality. An optimization over a long time horizon including both pulsing and gliding phases would be less meaningful due to the dynamically changing driving environment, not to mention the increased computation load. For online implementability, a series of approximations are applied as follows. The pulsing and gliding phase problems will then become quadratic.

*1) Linearization and Approximation of the Dynamics:* Based on the feature of small speed oscillation, the longitudinal dynamics (3) is linearized about the average speed of the PV, $\bar{v}$, to render

$$\dot{v} = 2k_1\bar{v}v - k_1\bar{v}^2 + k_2(T_e + T_m) - gf_r. \tag{12}$$

The absolute error of this linearization can be expressed as $|(2k_1\bar{v}v - k_1\bar{v}^2) - k_1v^2| = k_1\delta_v^2\bar{v}^2$, where $\delta_v := (v - \bar{v})/\bar{v}$ is the normalized speed deviation. In the simulations in Sec. V, the speed oscillations are set as 10%, so $\delta_v$ is 0.05 and $-0.05$ respectively for $v_{\max}$ and $v_{\min}$, where the maximum errors occur with the same values regardless the sign of $\delta_v$. The maximum relative error is expressed as $\delta_v^2/(1+\delta_v)^2$ and is 0.23% for 10% speed oscillations, for different average speeds. The maximum absolute errors to the vehicle acceleration in (12) due to linearization at different average speed for 10% speed oscillations are summarized in Table II. They increase

TABLE II: Maximum absolute error of vehicle speed linearization for 10% speed oscillation (unit: $1 \times 10^{-4}$ m/s$^2$)

| 30 mph | 40 mph | 50 mph | 60 mph | 70 mph |
|--------|--------|--------|--------|--------|
| 1.20 | 2.1 | 3.32 | 4.78 | 6.50 |
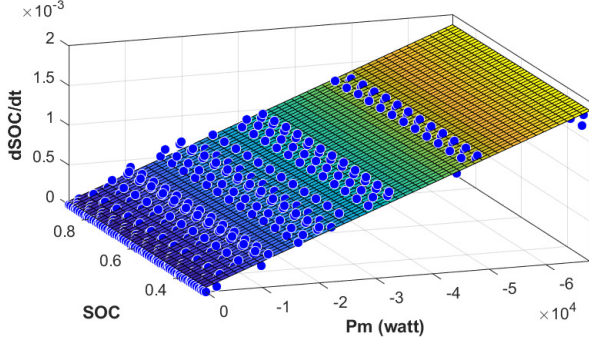


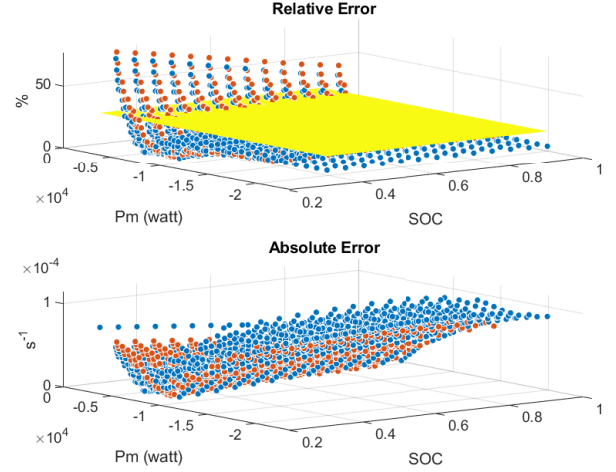Fig. 9: The linear approximation of the SOC dynamics while charging.



Fig. 10: The relative errors and absolute errors of the SOC dynamics approximation. The red and blue dots respectively represent the errors from over-estimates and under-estimates of the McCormick envelope. The yellow plane marks the 25% relative error. Beyond around $P_m = -3.5$ kW, the relative errors are less than 25%.

as the average speed increases but are all smaller than $1 \times 10^{-3}$ m/s$^2$.

For dealing with the nonlinearity of the SOC dynamics (4), the surface of $dSOC/dt$ during charging is approximated in both $SOC$ and $P_m$ with first order as shown in Fig. 9. The approximated SOC dynamics is

$$S\dot{O}C \approx c_{00} + c_{10}SOC + c_{01}P_m. \tag{13}$$

For the vehicle parameters used in this paper, the coefficients in (13) are $c_{00} = 7.919 \times 10^{-5}$, $c_{10} = -4.244 \times 10^{-5}$, and $c_{01} = -2.704 \times 10^{-8}$. However, $P_m = T_m\omega_m$ is in fact a bilinear term, so (13) is not yet linear. The motor power can be expressed in terms of vehicle speed as $P_m = c_{\omega v}T_m v$, where the coefficient $c_{\omega v} := r_T r_0/r_w$ is constant, because a fixed gear is used in our proposed method. Then the convex relaxation by the McCormick envelope approach [26] is adopted for $P_m$ as shown below.

The under-estimates of $P_m$ in terms of $T_m$ and $v$ are:

$$\begin{aligned} P_m &\geq (T_{m,\min}^{\text{ch}}v + T_m v_{\min} - T_{m,\min}^{\text{ch}}v_{\min})c_{\omega v} \\ P_m &\geq (T_{m,\max}^{\text{ch}}v + T_m v_{\max} - T_{m,\max}^{\text{ch}}v_{\max})c_{\omega v}, \end{aligned} \tag{14}$$

and the over-estimates of $P_m$ in terms of $T_m$ and $v$ are:

$$\begin{aligned} P_m &\leq (T_{m,\max}^{\text{ch}}v + T_m v_{\min} - T_{m,\max}^{\text{ch}}v_{\min})c_{\omega v} \\ P_m &\leq (T_m v_{\max} + T_{m,\min}^{\text{ch}}v - T_{m,\max}^{\text{ch}}v_{\max})c_{\omega v}. \end{aligned} \tag{15}$$

The motor power $P_m$ is added as yet another control variable in the pulsing phase problem in addition to $T_e$ and $T_m$. Now, the SOC dynamics approximated by (13) to (15) is linear.

The SOC approximation errors are analyzed as follows. As in the analysis of speed linearization errors, five average speeds from 30 mph to 70 mph are considered and used to compute their corresponding $v_{\max}$ and $v_{\min}$ (10% speed oscillations). The charging torque limits are $T_{m,\min}^{\text{ch}} = 0$ Nm and $T_{m,\max}^{\text{ch}} = -100$ Nm for analysis. With the bounds of vehicle speed and charging motor torque, the minimum under-estimates and maximum over-estimates of $P_m$ can be computed for every pair of vehicle speed and motor torque. Here only gear 6 is considered, because gear 6 gives higher MPG

improvement under the acceleration/deceleration constraints shown in Sec. V-A and is used in the simulations cases of varying speed PV.

The computed under-estimates and over-estimates of $P_m$ are then plugged into (13) with different SOC to compute the approximated $dSOC/dt$, the relative errors and absolute errors of which are shown in Fig. 10. When the charging power is beyond around $-3.5$ kW, the relative errors are less than 25%. When the charging power approaches zero, the relative errors are large since $dSOC/dt$ approaches zero as well. However, the absolute errors are less than $1 \times 10^{-4}$ s$^{-1}$, equivalent to contributing less than 0.01% SOC error in one second. Partitioning the domain of $SOC$ and $P_m$ to obtain better linear approximation of $dSOC/dt$ and/or using piecewise McCormick envelope to tighten the convex relaxation as in [31] can improve the SOC dynamics approximation, but at the expense of increasing the computation load. As observed in the simulations, the SOC sustenance is achieved, so the current approximation strategy for SOC dynamics is adopted. Also, the MPC control strategy adopted provides a feedback mechanism that offers certain robustness to the modeling errors.

*2) Relaxing the Acceleration/Deceleration Constraints:* Compared with keeping a proper range to the PV, which is about safety, the ride comfort constraints are less stringent and can be thus treated as soft ones. This relaxation of the acceleration/deceleration constraints can avoid the situation where feasible solutions are not able to converge to due to the PV varying its speed. Therefore, slack variables are added to the acceleration/deceleration constraints. For the sake of keeping computation load light, only the slack variable for the deceleration constraint is added in the gliding phase, and that for the acceleration constraint is added in the pulsing phase. It is because in the gliding phase the deceleration constraint is more crucial for safety, while in the pulsing the acceleration constraint is more stringent for keeping the desired range to

the PV.

Moreover, another control variable, the brake acceleration $a_b$, is introduced to provide the additional deceleration in the gliding phase. Here this brake acceleration is assumed to be achieved by the friction brake for simplicity, instead of modeling the regenerative braking. In fact, any kinds of braking is not desired in PnG, even for regenerative braking, because braking will consume the energy from engine, which is originally intended to drive the vehicle. Also, PnG is mainly a strategy for cruising scenarios without many stop-and-go events. Thus, regenerative braking is not considered in this paper.

The newly-introduced slack variables and the brake acceleration are penalized in the objective functions of the gliding and pulsing phase problems. The objective functions of (10) and (11) thus become:

$$\min_{T_m(t),s_d(t),a_b(t)} (t_{f,\text{gld}} - t_{0,\text{gld}}) + \int_{t_{0,\text{gld}}}^{t_{f,\text{gld}}} \left[ w_d s_d^2(t) + w_b a_b^2(t) \right] dt, \tag{16}$$

and

$$\min_{T_m(t),T_e(t),P_m(t),s_a(t)} (t_{f,\text{pls}} - t_{0,\text{pls}}) + \int_{t_{0,\text{pls}}}^{t_{f,\text{pls}}} w_a s_a^2(t) dt, \tag{17}$$

where $s_a$ and $s_d$ are respectively the slack variables of acceleration and deceleration constraints, $a_b \leq 0$ is the braking acceleration, and $w_a$, $w_d$, and $w_b$ are the associated weighting factors. Please note that $P_m$ is also one of the minimization arguments in (17) due to the McCormick envelope applied to the SOC dynamics explained above. In the proposed method, the gliding phase problem with (16) as the objective function will be solved as MPC in the gliding phase; the pulsing phase problem associated with (17) will be solved as MPC in the pulsing phase.

*3) Problem Convexification using Sparsity Optimization:* The PnG switching times, namely the $t_{f,\text{gld}}$ and $t_{f,\text{pls}}$ in Problems (10) and (11), are in fact unknown. If the unknown switching times are treated as variables, Problems (10) and (11) will become nonlinear due to the vehicle dynamics and the SOC dynamics, and the integration terms in (16) and (17) will become nonquadratic. In order to avoid this situation, the strategy based on sparsity optimization in [25] is utilized.

For completeness, the strategy in [25] is summarized as follows. Consider a discrete minimum-time control problem:

$$\min_{u(0),...,u(T-1)} T$$
$$\text{s.t.} \quad x(t+1) = Ax(t) + bu(t),$$
$$x(T) = 0 \text{ and } x(t) \neq 0, \ t = 0,1,...,T-1,$$
$$u(t) \in \mathscr{U}, \ t = 0,1,...,T-1. \tag{18}$$

It is equivalent to the sparsity optimization problem:

$$\min_{u(0),...,u(T-1)} |\{t : \|x(t)\|_2 \neq 0\}|$$
$$\text{s.t.} \quad x(t+1) = Ax(t) + bu(t),$$
$$\exists T_1 \leq T : x(t) = 0, \ t = T_1,...,T, \text{ and}$$
$$x(t) \neq 0, \ t = 0,1,...T_1 - 1,$$
$$u(t) \in \mathscr{U}, \ t = 0,1,...,T-1, \tag{19}$$

where the operator $\|(.)\|_2$ is the 2-norm and $|(.)|$ is the cardinality operator. Then with the increasing function $w(t)$ introduced, (19) is convexified as

$$\min_{u(0),...,u(T-1)} \sum_{t=1}^{T} w(t) \|x(t)\|_2$$
$$\text{s.t.} \quad x(t+1) = Ax(t) + bu(t),$$
$$u(t) \in \mathscr{U}, \ t = 0,1,...,T-1. \tag{20}$$

The problem of (20) is then solved using the MPC, of which the MPC horizon in fact does not need to cover the minimum time [25].

The approach of sparsity optimization for the minimum-time problems in [25] requires the target states to be at the origin. Therefore, the new states $\varepsilon_v := v - v_{\min}$ in the gliding phase and $\varepsilon_v := v - v_{\max}$ and $\varepsilon_{\text{soc}} := SOC - SOC_{\text{target}}$ in the pulsing phase, are defined. In summary, problems (10) and (11) become

$$\min_{T_m(t),s_d(t),a_b(t)} \int_{t_{0,\text{gld}}}^{t_{0,\text{gld}}+\Delta T_{\text{gld}}} \begin{bmatrix} w(t)\varepsilon_v(t)^2 + \\ w_d s_d^2(t) + w_b a_b^2(t) \end{bmatrix} dt$$
$$\text{s.t.} \quad d\dot{R}(t) = -(\varepsilon_v(t) + v_{\min}) + v_P + h_\tau a_P$$
$$\dot{\varepsilon}_v(t) = 2k_1\bar{v}(\varepsilon_v(t) + v_{\min}) - k_1\bar{v}^2 + \\ k_2 T_m(t) - gf_r - a_b$$
$$a_{\lim} \geq a(t) \geq -d_{\lim} - s_d(t)$$
$$0 \leq T_m(t) \leq T_{m,\max}^{\text{disch}}$$
$$\dot{T}_{m,\min} \leq \dot{T}_m(t) \leq \dot{T}_{m,\max}$$
$$dR_{\min} \leq dR(t) \leq dR_{\max}$$
$$s_d(t) \geq 0$$
$$a_b(t) \leq 0, \tag{21}$$

and

$$\min_{\substack{T_m(t),T_e(t); \\ P_m(t),s_a(t)}} \int_{t_{0,\text{pls}}}^{t_{0,\text{pls}}+\Delta T_{\text{pls}}} \left\{ \begin{array}{l} w(t)\left[\varepsilon_v^2(t) + w_{\text{soc}}\varepsilon_{\text{soc}}^2(t)\right] + \\ w_a s_a^2(t) \end{array} \right\} dt$$
$$\text{s.t.} \quad d\dot{R}(t) = -(\varepsilon_v(t) + v_{\max}) + v_P + h_\tau a_P$$
$$\dot{\varepsilon}_v(t) = 2k_1\bar{v}(\varepsilon_v(t) + v_{\max}) - k_1\bar{v}^2 + \\ k_2(T_e(t) + T_m(t)) - gf_r$$
$$\dot{\varepsilon}_{\text{soc}}(t) = c_{00} + c_{10}(\varepsilon_{\text{soc}} + SOC_{\text{target}}) + c_{01}P_m(t)$$
$$P_m(t) \geq \begin{bmatrix} T_{m,\min}^{\text{ch}}(\varepsilon_v(t) + v_{\max}) \\ + T_m(t)v_{\min} - T_{m,\min}^{\text{ch}}v_{\min} \end{bmatrix} c_{\omega v}$$
$$P_m(t) \geq \begin{bmatrix} T_{m,\max}^{\text{ch}}(\varepsilon_v(t) + v_{\max}) \\ + T_m(t)v_{\max} - T_{m,\max}^{\text{ch}}v_{\max} \end{bmatrix} c_{\omega v}$$
$$P_m(t) \leq \begin{bmatrix} T_{m,\max}^{\text{ch}}(\varepsilon_v(t) + v_{\max}) \\ + T_m(t)v_{\min} - T_{m,\max}^{\text{ch}}v_{\min} \end{bmatrix} c_{\omega v}$$
$$P_m(t) \leq \begin{bmatrix} T_{m,\min}^{\text{ch}}(\varepsilon_v(t) + v_{\max}) \\ + T_m(t)v_{\max} - T_{m,\max}^{\text{ch}}v_{\max} \end{bmatrix} c_{\omega v}$$
$$-d_{\lim} \leq a(t) \leq a_{\lim} + s_a(t)$$
$$T_{m,\max}^{\text{ch}} \leq T_m(t) \leq 0$$
$$\dot{T}_{m,\min} \leq \dot{T}_m(t) \leq \dot{T}_{m,\max}$$
$$0 \leq T_e(t) \leq \bar{T}_{\text{sw}}$$
$$\dot{T}_{e,\min} \leq \dot{T}_e(t) \leq \dot{T}_{e,\max}$$
$$0 \leq T_e(t) + T_m(t)$$
$$dR_{\min} \leq dR(t) \leq dR_{\max}$$
$$s_a(t) \geq 0, \tag{22}$$

where $\Delta T_i$, $i \in \{\mathrm{gld}, \mathrm{pls}\}$, is the MPC horizon, and $w_{\mathrm{soc}}$ in the objective function of (22) is the weighting factor for balancing the magnitudes of $\varepsilon_v$ and $\varepsilon_{\mathrm{soc}}$. The increasing function $w(t)$ from the sparsity optimization approach in [25] is defined as

$$w(t) = \alpha(t - t_{0,i}), \qquad (23)$$

where $\alpha > 0$ is a constant and $t_{0,i}$, $i \in \{\mathrm{gld}, \mathrm{pls}\}$, is the current time.

*4) Applying the Pseudo-Spectral Method:* With the linearization and approximation techniques introduced above, Problems (21) and (22) are now with quadratic objective functions, and their dynamics and constraints are all linear. The PS method is then used to transcribe them. The resultant QP problems can be solved efficiently using existing solvers.

In summary, during the gliding phase, (21) is solved until the switching criterion is met. Then the vehicle enters the pulsing phase and starts solving (22) until the switching criterion is met to switch to the gliding phase again. The switching criterion is set as $dR = 0$ with $v < \bar{v}$ in gliding and $v > \bar{v}$ in pulsing. This way, the trivial solutions that lead to immediate PnG switching can be avoided.

In the simulation studies of this paper, the PV trajectories of the speed and acceleration are assumed to be available in the MPC horizons. In practical applications, proper prediction methods, such as those in [32] and [33] can be used to provide this information. The predication capability and the onboard computation power need to be considered together to decide a suitable MPC horizon, which is out of the scope of this work.

### C. Ride Comfort Requirement

In this paper, only the pulsing acceleration and gliding deceleration are considered explicitly for ride comfort. At the moments of phase switching where large jerks may occur, it is assumed that the jerks can be alleviated using the proper design of low-level actuator control.

In general, the periods of PnG cycles are at the order of ten seconds. However, the research of motion sickness under such low frequencies of vibration is not readily available in literature. Most of the research efforts cover the excitation frequencies down to only 0.1 Hz or are not for the longitudinal direction [34], [35]. To overcome this limitation, the Safety Pilot dataset [28] is resorted to in deducing the level of acceleration that drivers experience in daily car-following scenarios.

The data of car-following scenarios in the Safety Pilot dataset is focused. Specifically, the events with less than 10% speed variation are extracted. These events range from 30 to 80 mph with root-mean-square (RMS) acceleration from 0.17 to 0.2 m/s$^2$. We then choose 0.2 m/s$^2$, though possibly conservative, as the acceleration/deceleration limits for the ride comfort requirement, close to the suggested value of 0.3 m/s$^2$ in [24].

### V. SIMULATION RESULTS

A series of numerical simulations using the proposed method are presented here. For the purpose of understanding the fuel saving potentials with different PnG operations, the
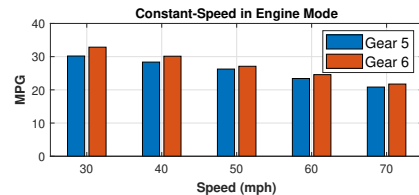


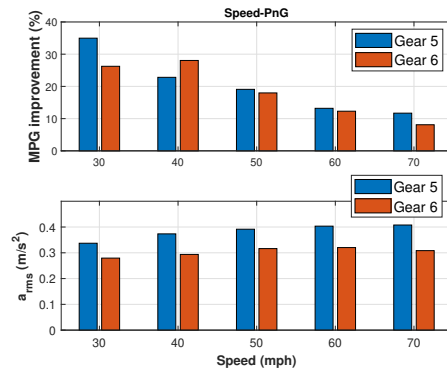Fig. 11: The fuel economy of constant speed in engine mode without PnG at different speeds.



Fig. 12: The improvements of fuel economy and RMS accelerations of Speed-PnG with 10% speed oscillation at different speeds. Baseline: constant-speed driving in engine mode with gear 6.

cases using different energy buffers with constant PV speeds are studied. Then the proposed method is further applied to a case of PV with varying speed to test its performance. Finally, the Safety Pilot dataset is utilized to gain the statistical understanding of how the proposed approach performs in naturalistic driving scenarios. All cases are assumed to be without any road grade variation, and the FV starts the PnG car-following process with the desired range to the PV. As it will be seen that gear 6 always renders better fuel economy in SOC-PnG with speed oscillations from the study of constant-speed PV cases, in the cases with varying PV speed, including the study using the Safety Pilot dataset, gear 6 is used. The MPC horizons for all cases are set as 6 s, which corresponds to the maximum absolute prediction error about 0.8 m/s in [36] using the artificial neural network method. We use the MATLAB built-in quadprog solver to solve the transcribed MPC optimization problems. The computation time for each optimization problem is less than 0.1 s on a laptop with Intel® i5 CPU in MATLAB. The computation efficiency can be even higher if using a high-level general purpose programming language like C language. Therefore, the developed controller is online implementable, since $\Delta T$ is chosen as 0.5 s, i.e., solving the MPC as QP problems every 0.5 s, which is sufficient for normal driving situations.

### A. Constant-Speed Preceding Vehicle

Due to the nonlinear characteristics of ICE engines, specifically the concave-convex shape of fuel rate curve in Fig. 1, maintaining a constant engine output may not be the most fuel-economical way of driving in cruising. Figures 11 and 12 are respectively the MPG for constant-speed driving entirely in engine mode and improvements of fuel economy from
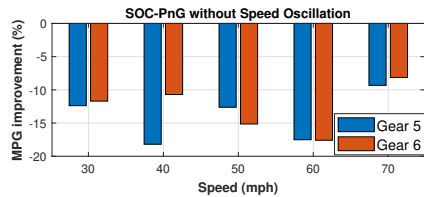
Fig. 13: The improvements of fuel economy with pure SOC-PnG at different speeds. Pure SOC-PnG cannot lead to fuel saving for the vehicle studied due to the high ohmic loss during the battery charging and discharging. Baseline: constant-speed driving in engine mode with gear 6.
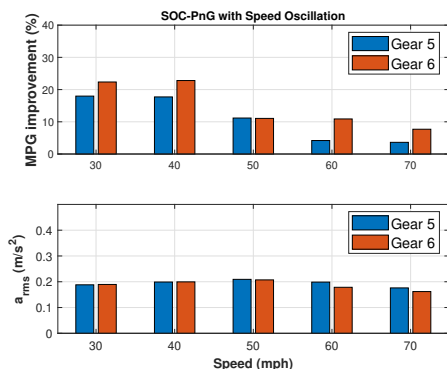


Fig. 14: The improvements of fuel economy and RMS accelerations of SOC-PnG with 10% speed oscillation at different speeds. The fuel saving potentials are partially regained with reduced RMS accelerations (increased ride comfort) compared with the cases of pure Speed-PnG. Baseline: constant-speed driving in engine mode with gear 6.
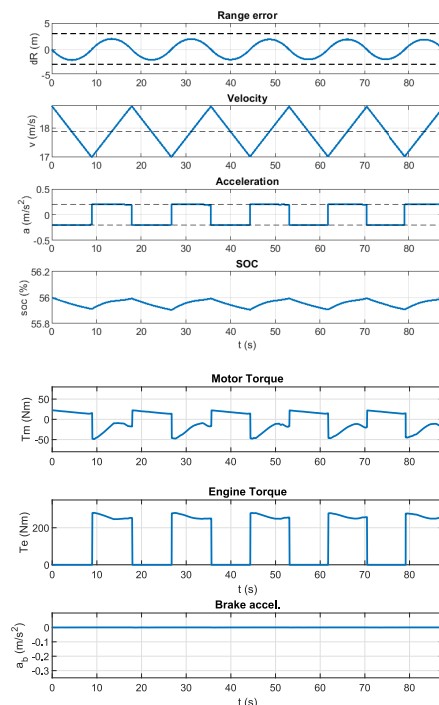


Fig. 15: The simulation trajectories of the case with constant-speed PV at 40 mph. The transmission is at gear 6. The dashed lines from top to bottom are the allowed range error, PV speed, and acceleration and deceleration constraints for ride comfort.

Speed-PnG with 10% speed oscillation. The improvements of fuel economy are computed against the results of constant-speed in engine mode with gear 6 at corresponding speeds, since gear 6 gives higher MPG as shown in Fig. 11. It can be seen that Speed-PnG leads to the improvements of fuel economy ranging from around 8% to 35%. The results of fuel saving of Speed-PnG gradually decrease with the increase of speed. When the vehicle speed increases, the benefit of PnG gradually decreases as suggested in Fig. 1, i.e., the gradual convergence of $Q_{PnG}$ to $Q_{CS}$. However, the significant fuel savings of Speed-PnG come with the price of sacrificing the ride comfort. Also shown in Fig. 12 are the RMS accelerations of Speed-PnG under different speeds. They can be as high as 0.4 m/s$^2$ if gear 5 is used.

On the other hand, SOC-PnG uses the battery as the energy buffer, so better ride comfort can be ensured. Here $SOC_{max} = 57\%$ and $SOC_{min} = 55\%$ define the SOC range for SOC-PnG. The motor drives the vehicle to maintain the constant speed until $SOC_{min}$ is reached, and then the engine is turned on to both drive the vehicle and charge the battery to $SOC_{max}$ at the same time. The former and latter phases are repeated alternately and can be respectively seen as the gliding phase and pulsing phase for SOC-PnG. Figure 13 shows the results. Even though SOC-PnG can maintain constant speed, the vehicle studied in this paper cannot benefit from it for fuel saving due to the high vehicle weight and high loss during battery charging/discharging.

With the purpose of combining the high fuel saving potential of Speed-PnG and the ride comfort capability of SOC-PnG, the

proposed method is applied to introduce 10% speed oscillation to SOC-PnG at different speeds. The results are summarized in Fig. 14. The SOC-PnG with speed oscillation recovers partially the fuel saving potential and leads to the improvements of fuel economy ranging from about 22.4% to 4%. More importantly, the resulted RMS accelerations are around 0.2 m/s$^2$, the level of acceleration/deceleration limits assigned for ride comfort. As an example, the simulation trajectories of SOC-PnG with 10% speed oscillation at 40 mph are shown in Fig. 15. The range error, speed, and SOC are oscillatory and maintained around their average values as the engine is turned on and off alternately, with both the vehicle body and the battery being involved as the energy buffers. In the pulsing phase, the engine power drives the vehicle with the acceleration limit adhered to while charging the battery. In the gliding phase, the engine is turned off and the motor is turned on to provide some driving power such that the deceleration limit is satisfied.

Through this study, it is shown that the proposed method is able to simultaneously leverage both the temporary energy buffers, namely, the vehicle body and the battery, to improve the fuel economy while considering ride comfort and SOC sustenance. As discussed in Sec. III, the vehicle body is a much more efficient energy buffer compared with the battery, so conceptually pure Speed-PnG sets the upper bound and pure SOC-PnG sets the lower bound of the fuel saving potential achievable. The proposed method is to achieve a balance in between.

Next, the proposed method is applied to a case with varying-speed PV to further examine its performance.
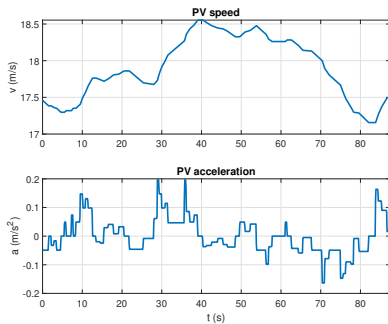
Fig. 16: The speed and acceleration trajectories of the PV in the case of varying-speed PV.

## B. Varying-Speed Preceding Vehicle

The speed and acceleration profiles of PV in this case study are shown in Fig. 16. The PV travels around 40 mph with 0.06 m/s$^2$ RMS acceleration, and the instantaneous acceleration sometimes reaches 0.2 m/s$^2$. Two cases, one with the FV starting with pulsing and another one starting with gliding, are simulated. The baseline is driving in engine mode with the PV speed profile in gear 6. The achieved fuel economy is respectively 36.6 MPG and 40.9 MPG, with the one starting in pulsing slightly lower. In the cases of constant PV speeds presented above in Sec. V-A, complete full PnG cycles are extracted to compute the MPG results. In real applications, we might not be able to have complete full PnG cycles. If the vehicle is in the gliding phase more, the fuel economy will be better. Therefore, the initial PnG phases would influence how much fuel can be saved, especially for short travelling distance. Compared with the 29.3 MPG of engine mode without using PnG, around 32.1% MPG improvement can be achieved if the average of the cases of starting with pulsing and with gliding is considered.

Figures 17 and 18 are the trajectories of the two cases with different initial PnG phases. We can see that in both cases the FV travels with speed oscillating around the PV speed and the range error satisfies the preset limit. However, the acceleration sometimes exceeds the acceleration/deceleration limits for ride comfort. It is because the PV now in this case is not constant, and the FV sometimes needs to increase its acceleration or deceleration momentarily to maintain a proper distance to the PV. For example, at about $t = 32$ s in Fig. 17, the FV increase its acceleration beyond 0.2 m/s$^2$, the preset limit, so that later at $t = 38$ s the range error constraint is not violated. Also, at $t = 46$ s in Fig. 18, the FV increases its deceleration a little beyond the deceleration limit, so that the range error does not violate the lower bound right after. This behavior results in 0.22 m/s$^2$ and 0.23 m/s$^2$ RMS acceleration for the cases in Fig. 17 and Fig. 18, respectively, slightly above the preset limit 0.2 m/s$^2$.

The simulations in this case study demonstrate the capability of the proposed method to adjust its acceleration in response to the PV's varying speed, which is important in real applications. Further study to obtain the statistical performance of the proposed method using naturalistic driving data is presented next.
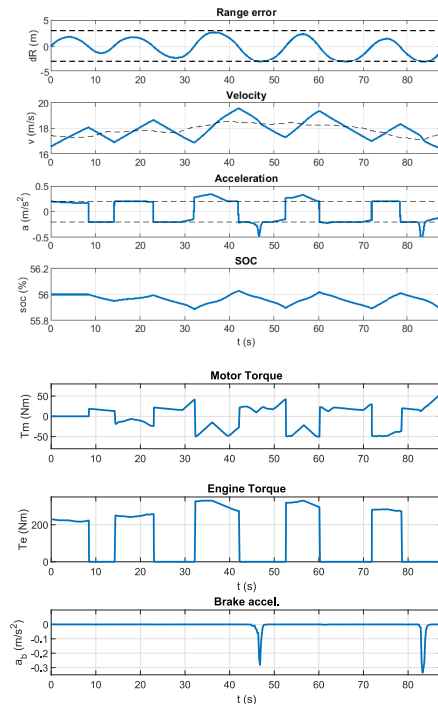


Fig. 17: The simulation trajectories of the case of varying-speed PV at 40 mph and starting in pulsing. The transmission is at gear 6. The dashed lines from top to bottom are the allowed range error, PV speed, and acceleration and deceleration constraints for ride comfort.
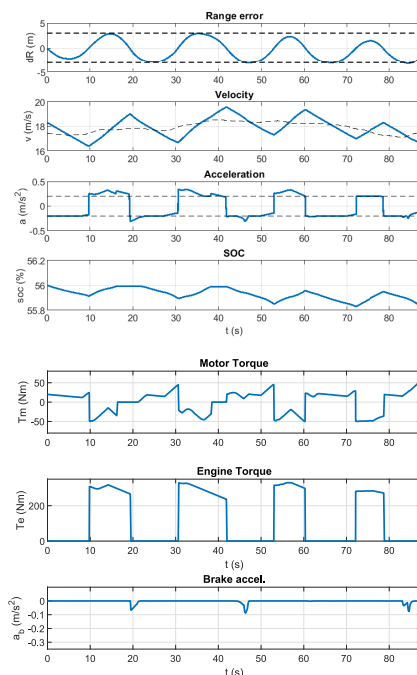


Fig. 18: The simulation trajectories of varying-speed PV at 40 mph and starting in gliding. The transmission is at gear 6. The dashed lines from top to bottom are the allowed range error, PV speed, and acceleration and deceleration constraints for ride comfort.

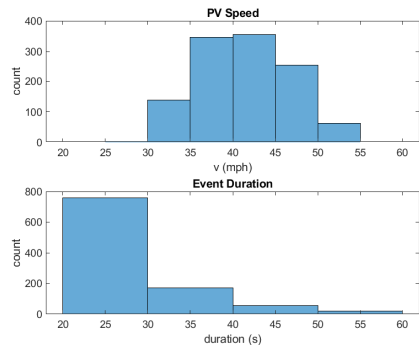## C. Naturalistic-Speed Preceding Vehicle



Fig. 19: The statistics of the events extracted from the Safety Pilot dataset used in the simulations for local roads. The events are of less than 10% speed variation.

The Safety Pilot dataset is leveraged to define the PV speed in this case study. In total 1,161 events of local roads and 507 events of highways in cruising scenarios, each with speed variation less than 10%, are extracted. They amount to 8.5 hours and 11.4 hours of driving respectively on local roads and highways. The distributions of the speed and duration are shown in Fig. 19 and Fig. 21 for local and highway events, respectively. Like the study in Sec. V-B, two simulations are conducted for each event, one starting with the FV in pulsing and another in gliding, and the average improvement of fuel economy of these two represents the MPG result of this specific event. The baseline is also driving in engine mode with the PV speed profile in gear 6.

Figures 20 and 22 respectively summarize the results of local events and highway events. First, we can see that on average the FV has RMS accelerations pushed to be higher than 0.2 m/s$^2$, due to the accelerations of PV. Moreover, for some events, PnG actually even leads to more fuel consumption, as indicated by negative MPG improvements in both Fig. 20 and Fig. 22.

For comparison, the adaptive cruise control (ACC) and cooperative adaptive control (CACC) approaches in [37] are also implemented using the same driving data for the PV. In [37], the acceleration of the FV in ACC is based on the proportional-derivative (PD) feedback control:

$$a_{\text{ACC}} = K_P(R - R_{\text{des}}) + K_D \frac{d}{dt}(R - R_{\text{des}}), \qquad (24)$$

where $K_P$ and $K_D$ are the proportional and derivative gains. The FV acceleration in CACC is simply with the feedfoward term $a_P$ added:

$$a_{\text{CACC}} = K_P(R - R_{\text{des}}) + K_D \frac{d}{dt}(R - R_{\text{des}}) + a_P, \qquad (25)$$

where $a_P$ is the acceleration of PV, which is transmitted via inter-vehicle communication. In the simulations, $K_P = 0.64$ and $K_D = 0.8$ are used, same as those in [37], and the vehicle is operated in gear 6. The speed and acceleration trajectories of the FV result from (24) and (25) are used to compute the required driving torque. Then the fuel consumption in hybrid mode of each event is obtained.
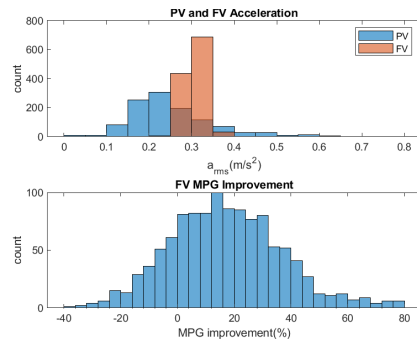


Fig. 20: The statistics of the simulation results of RMS accelerations and improvements of fuel economy using the Safety Pilot dataset on local roads.
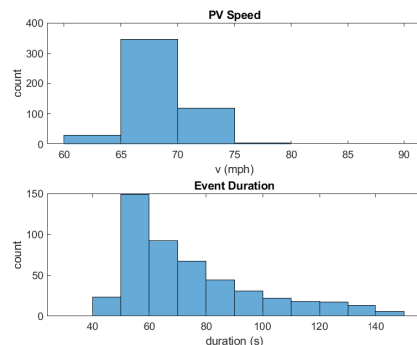


Fig. 21: The statistics of the events extracted from the Safety Pilot dataset used in the simulations for highways. The events are of less than 10% speed variation.

To find out the fuel saving potential of ACC and CACC in hybrid mode for the vehicle studied in this paper, the dynamic programming approach is applied. The formulated dynamic programming is to minimize the fuel consumption given the trajectory of required driving torque in each event. The state is the battery SOC and the control is the motor torque. The final SOC is enforced to equal the initial SOC, which is 56%, the same value as in the PnG cases. Then the engine torque is decided based on the required driving torque and the fuel consumption is computed.

Table III summarizes the statistics of MPG improvement using the proposed method, ACC, and CACC. For the proposed method, the MPG improvement on average is 17.1% with standard deviation 19.9% for local events and 5.1% with standard deviation 5.5% for highway events. ACC on average achieves 5.8% MPG improvement with 12.0% standard deviation on local roads. As to CACC, knowing the PV acceleration via inter-vehicle communication helps avoid the drastic acceleration and deceleration compared with ACC, reaching 7.3% MPG

TABLE III: The mean value and standard deviation of MPG improvements using the Safety Pilot dataset (unit: %)

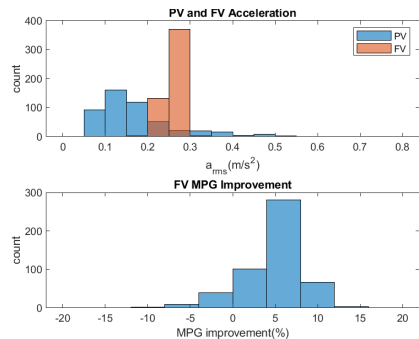|  | PnG (proposed) | | ACC ([37]) | | CACC ([37]) | |
|---|---|---|---|---|---|---|
|  | local | highway | local | highway | local | highway |
| mean value | 17.1 | 5.1 | 5.8 | 1.5 | 7.3 | 1.6 |
| standard deviation | 19.9 | 5.5 | 12.0 | 3.1 | 11.8 | 2.8 |

Fig. 22: The statistics of the simulation results of RMS accelerations and improvements of fuel economy using the Safety Pilot dataset on highways.
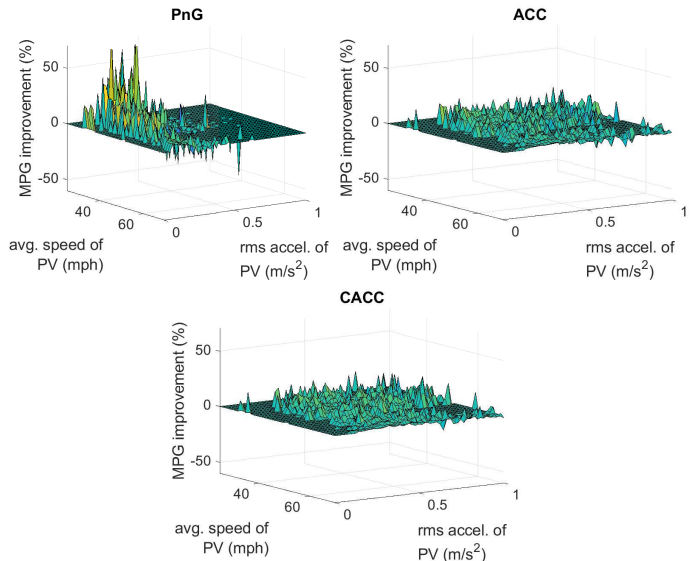


Fig. 23: The distribution of MPG improvements over PV average speed and PV RMS accelerations using the Safety Pilot data for all the local and highway events.

improvement with 11.8% standard deviation on local roads. On highways, the benefit of knowing the PV acceleration becomes less significant, because highway driving is usually smooth without drastic variations of acceleration and deceleration. Therefore, there is no significant difference between the ACC and CACC statistics. They achieve 1.5% with 3.1% standard deviation and 1.6% with 2.8% standard deviation, respectively. The simulation results suggest that PnG has higher fuel saving potential compared with ACC and CACC during cruising.

Figure 23 plots the MPG improvements against the PV average speed and PV RMS acceleration for all the local and highway events. Most of the cases with PnG can save significant amount of fuel at lower speeds and lower PV accelerations.However, when the PV acceleration increases, PnG may lead to more fuel consumption. As shown in Sec. V-B, the FV sometimes needs to apply brake in order to maintain the distance to the varying-speed PV. This situation of brake application would happen more frequently if the PV accelerates and decelerates more drastically, and thus increases the fuel consumption. This is also true for the regenerative braking, since the regenerative braking can only partially capture the energy back. On the other hand, ACC may have the chance to reduce the fuel consumption when the PV accelerations are large. If the vehicles are equipped with the inter-vehicle communication, CACC may even improve the fuel economy in this situation. On highways, the fuel saving potential of PnG is small already, not to mention when the PV accelerations are high. Thus, in situations of high speed with large PV accelerations, ACC or CACC may be better options.

From this study using the Safety Pilot dataset, some PnG cases that even consume more fuel than the baseline are observed. It happens more often when the PV accelerations are larger. If the sweet spot of the engine has not been reached, the driver can choose to sacrifice the ride comfort in exchange for fuel saving in this situation. Also, the driver can follow the PV with a longer distance, so the FV's PnG operation can be less affected. Switching to ACC or CACC could be another option. Therefore, a sophisticated high-level decision maker is needed to determine the proper car-following strategies and to adjust the PnG parameters in different situations. Also, when the PV acceleration is larger, the time horizon that can give accurate prediction of PV behaviors is shorter. The MPC

horizon is to be shortened accordingly in this situation to have meaningful solutions. How this will impact the performance of the proposed method and how to determine a proper MPC horizon in accordance with the traffic is also an important remaining research task.

## VI. CONCLUSION

In this paper, an online implementable MPC controller is proposed for PnG operations of HEVs in car-following scenarios. This MPC controller leverages the two energy buffers of HEVs, namely the vehicle body and the battery, to reach a balance between fuel economy and ride comfort, while maintaining SOC. Specifically, two minimum-time optimal control problems are formulated in the proposed method, one for pulsing and another for gliding. For setting the ride comfort requirements in these two control problems, the Safety Pilot dataset is analyzed. The obtained RMS acceleration of 0.2 m/s$^2$ in car-following scenarios is used to define the acceleration/deceleration constraints for ride comfort. Then via the linearization of vehicle dynamics, the convexification using the McCormick envelope for the approximated SOC dynamics, and the method of sparsity optimization in [25], these two minimum-time control problems become linear with quadratic costs. Therefore, they can be solved as QP problems efficiently after being transcribed by the PS method.

In the numerical simulations with constant-speed PV, about 4% to 22.4% MPG improvements are achieved from 30 to 70 mph, with the general trend that MPG improvements decrease with the increase of speed. The capability of recovering the fuel saving potential by introducing speed oscillations to SOC-PnG is thus demonstrated. In the simulations using the Safety Pilot dataset, the average MPG improvements observed are about 17.1% from the 8.5 hour data on local roads and 5.1% from the 11.4 hour data on highways, higher than those achieved by car-following using ACC (5.8% on local roads

and 1.5% on highways) and CACC (7.3% on local roads and 1.6% on highways). These results show that PnG has higher fuel saving potential during cruising compared with ACC and CACC. The exact fuel saving performance of PnG depends on the characteristics of individual powertrain and vehicle parameters. However, based on the simulation results, the proposed framework is a promising approach to realize the optimal PnG operations on HEVs by balancing the benefits of Speed-PnG and SOC-PnG, i.e., fuel saving and ride comfort, respectively.

In the simulations using the Safety Pilot dataset, there are some cases that PnG cannot save fuel, especially for those with large PV accelerations. In these situations, using ACC or CACC could be an option for fuel saving and ride comfort. This suggests that a higher-level decision making strategy is needed to leverage the fuel saving potential of PnG properly. This higher-level strategy for PnG operations should consider concurrently the ride comfort preferences of the driver and the PV's behaviors in determining the proper PnG parameters and the range policy, as well as the MPC horizon. Other limitations of the current work include the robustness under uncertainties such as road grade variation and the variation of aerodynamic drag due to close car-following. Addressing these limitations is for future work.

## REFERENCES

[1] National Highway Traffic Safety Administration, *Corporate Average Fuel Economy Standards for Model Years 2024-2026 Passenger Cars and Light Trucks*, https://www.govinfo.gov/content/pkg/FR-2022-05-02/pdf/2022-07200.pdf.

[2] E. G. Gilbert, "Vehicle cruise: Improved fuel economy by periodic control," 1976.

[3] J. Lee, "Vehicle inertia impact on fuel consumption of conventional and hybrid electric vehicles using acceleration and coast driving strategy," Ph.D. dissertation, Virginia Tech, 2009.

[4] B. Jawad, E. Marck, D. Tingley, T. Salvati, J. McCoy, A. Ondes, E. Poota, and V. Floma, "Best practices for an sae supermileage® vehicle," SAE Technical Paper, Tech. Rep., 2001.

[5] S. E. Li and H. Peng, "Strategies to minimize the fuel consumption of passenger cars during car-following scenarios," *Proceedings of the Institution of Mechanical Engineers, Part D: Journal of Automobile Engineering*, vol. 226, no. 3, pp. 419–429, 2012.

[6] S. E. Li, H. Peng, K. Li, and J. Wang, "Minimum fuel control strategy in automated car-following scenarios," *IEEE Transactions on Vehicular Technology*, vol. 61, no. 3, pp. 998–1007, 2012.

[7] S. E. Li, Q. Guo, L. Xin, B. Cheng, and K. Li, "Fuel-saving servo-loop control for an adaptive cruise control system of road vehicles with step-gear transmission," *IEEE Transactions on Vehicular Technology*, vol. 66, no. 3, pp. 2033–2043, 2016.

[8] J. Kim and C. Ahn, "Real-time speed trajectory planning for minimum fuel consumption of a ground vehicle," *IEEE Transactions on Intelligent Transportation Systems*, vol. 21, no. 6, pp. 2324–2338, 2019.

[9] Y. Imanishi, N. Tashiro, Y. Iihoshi, and T. Okada, "Development of predictive powertrain state switching control for eco-saving acc," SAE Technical Paper, Tech. Rep., 2017.

[10] S. E. Li, X. Hu, K. Li, and C. Ahn, "Mechanism of vehicular periodic operation for optimal fuel economy in free-driving scenarios," *IET Intelligent Transport Systems*, vol. 9, no. 3, pp. 306–313, 2014.

[11] S. Bittanti, G. Fronza, and G. Guardabassi, "Periodic control: A frequency domain approach," *IEEE Transactions on Automatic Control*, vol. 18, no. 1, pp. 33–38, 1973.

[12] W. Cao, T. Yuno, and T. Kawabe, "Pulse and glide strategy analysis based on engine operating point during pulse mode," *European Journal of Control*, vol. 65, p. 100629, 2022.

[13] K. Mcdonough, I. Kolmanovsky, D. Filev, D. Yanakiev, S. Szwabowski, and J. Michelini, "Stochastic dynamic programming control policies for fuel efficient vehicle following," in *2013 American Control Conference*. IEEE, 2013, pp. 1350–1355.

[14] R. Schmied, H. Waschl, and L. Del Re, "Extension and experimental validation of fuel efficient predictive adaptive cruise control," in *2015 American Control Conference (ACC)*. IEEE, 2015, pp. 4753–4758.

[15] V. Turri, O. Flärdh, J. Mårtenssont, and K. H. Johansson, "Fuel-optimal look-ahead adaptive cruise control for heavy-duty vehicles," in *2018 Annual American Control Conference (ACC)*. IEEE, 2018, pp. 1841–1848.

[16] J. Han, A. Vahidi, and A. Sciarretta, "Fundamentals of energy efficient driving for combustion engine and electric vehicles: An optimal control perspective," *Automatica*, vol. 103, pp. 558–572, 2019.

[17] Y. Chen and M. Lazar, "Real-time driving mode advice for eco-driving using mpc," *IFAC-PapersOnLine*, vol. 53, no. 2, pp. 13 830–13 835, 2020.

[18] J. Zhu, C. Ngo, and A. Sciarretta, "Real-time optimal eco-driving for hybrid-electric vehicles," *IFAC-PapersOnLine*, vol. 52, no. 5, pp. 562–567, 2019.

[19] K. M. So, P. Gruber, D. Tavernini, A. E. H. Karci, A. Sorniotti, and T. Motaln, "On the optimal speed profile for electric vehicles," *IEEE Access*, vol. 8, pp. 78 504–78 518, 2020.

[20] Z. Tian, L. Liu, and W. Shi, "A pulse-and-glide-driven adaptive cruise control system for electric vehicle," *International Transactions on Electrical Energy Systems*, vol. 31, no. 11, p. e13054, 2021.

[21] S. Xu, S. E. Li, H. Peng, B. Cheng, X. Zhang, and Z. Pan, "Fuel-saving cruising strategies for parallel hevs," *IEEE Transactions on vehicular technology*, vol. 65, no. 6, pp. 4676–4686, 2015.

[22] C. Whitehair and H. Denlinger, Michelleand Fathy, "Pulse-and-glide driving with drivability constraints: A pontryagin approach," 2018.

[23] C. Sohn, J. Andert, and R. N. N. Manfouo, "A driveability study on automated longitudinal vehicle control," *IEEE Transactions on Intelligent Transportation Systems*, 2019.

[24] C. Sohn, J. Andert, and D. Jolovic, "An analysis of the tradeoff between fuel consumption and ride comfort for the pulse and glide driving strategy," *IEEE Transactions on Vehicular Technology*, 2020.

[25] L. Bako, D. Chen, and S. Lecoeuche, "A numerical solution to the minimum-time control problem for linear discrete-time systems," *arXiv preprint arXiv:1109.3772*, 2011.

[26] G. P. McCormick, "Computability of global solutions to factorable nonconvex programs: Part i—convex underestimating problems," *Mathematical programming*, vol. 10, no. 1, pp. 147–175, 1976.

[27] S.-Y. Shieh, T. Ersal, and H. Peng, "Pulse-and-glide operation for parallel hybrid electric vehicles with step-gear transmission in automated car-following scenario with ride comfort consideration," in *2019 American Control Conference (ACC)*. IEEE, 2019, pp. 959–964.

[28] D. Bezzina and J. Sayer, "Safety pilot model deployment: Test conductor team report," *Report No. DOT HS*, vol. 812, no. 171, p. 18, 2014.

[29] F. Fahroo and I. M. Ross, "Advances in pseudospectral methods for optimal control," in *AIAA guidance, navigation and control conference and exhibit*, 2008, p. 7309.

[30] M. A. Patterson and A. V. Rao, "Gpops-ii: A matlab software for solving multiple-phase optimal control problems using hp-adaptive gaussian quadrature collocation methods and sparse nonlinear programming," *ACM Transactions on Mathematical Software (TOMS)*, vol. 41, no. 1, p. 1, 2014.

[31] P. M. Castro, "Tightening piecewise mccormick relaxations for bilinear problems," *Computers & Chemical Engineering*, vol. 72, pp. 300–311, 2015.

[32] F. Han, Y. Tan, and J. Eledath, "Preceding vehicle trajectory prediction by multi-cue integration." in *MVA*, 2007, pp. 575–578.

[33] R. Pandita and D. Caveney, "Preceding vehicle state prediction," in *2013 IEEE Intelligent Vehicles Symposium (IV)*. IEEE, 2013, pp. 1000–1006.

[34] M. J. Griffin and J. Erdreich, "Handbook of human vibration," 1991.

[35] ISO, "Evaluation of human exposure to whole-body vibration - part 3: Evaluation of exposure to whole-body z-axis vertical vibration in the frequency range 0.1 to 0.63 hz," vol. ISO 2631/3-1985(E), 1985.

[36] S. Lefèvre, C. Sun, R. Bajcsy, and C. Laugier, "Comparison of parametric and non-parametric approaches for vehicle speed prediction," in *2014 American Control Conference*. IEEE, 2014, pp. 3494–3499.

[37] G. J. Naus, R. P. Vugts, J. Ploeg, M. J. van De Molengraft, and M. Steinbuch, "String-stable cacc design and experimental validation: A frequency-domain approach," *IEEE Transactions on vehicular technology*, vol. 59, no. 9, pp. 4268–4279, 2010.

**Su-Yang Shieh** received the B.E.S. and M.S. degrees from the National Taiwan University, Taipei, Taiwan, in 2007 and 2009, respectively, and the Ph.D degree in 2021 in the Department of Mechanic, University of Michigan, Ann Arbor, MI USA, all in mechanical engineering. MI USA. He currently is a researcher with the General Motors Technical Center, Warren, MI. His research interests include decentralized control, network optimization, and stochastic control, with applications to power systems and transportation systems.

**Tulga Ersal** received the B.S.E. degree from the Istanbul Technical University, Istanbul, Turkey, in 2001, and the M.S. and Ph.D. degrees from the University of Michigan, Ann Arbor, MI USA, in 2003 and 2007, respectively, all in mechanical engineering. He is currently an Associate Research Scientist in the Department of Mechanical Engineering, University of Michigan, Ann Arbor, MI. His research interests include modeling, simulation, and control of dynamic systems, with applications to energy and transportation systems and biomechanics. Dr. Ersal is a member of the American Society of Mechanical Engineers.

**Huei Peng** received the Ph.D. degree in mechanical engineering from the University of California at Berkeley, Berkeley, CA, USA, in 1992. He was a Professor with the Department of Mechanical Engineering, University of Michigan, Ann Arbor, MI, USA. He was also a Chang Jiang Scholar with Tsinghua University, Beijing, China. His research interests included adaptive control and optimal control, with an emphasis on their applications to vehicular and transportation systems, design and control of electrified vehicles, and connected/automated vehicles. Dr. Peng was a fellow of the Society of Automotive Engineers and the American Society of Mechanical Engineers.